Research Square

Preprints are preliminary reports that have not undergone peer review.
They should not be considered conclusive, used to inform clinical practice,
or referenced by the media as validated information.

CD38 Drives Cellular Senescence and Ischemia-Reperfusion Injury in Donor Lungs

Dhiaeddine Djabri

dhiaeddine.djabri@osumc.edu

The Ohio State University https://orcid.org/0009-0007-9121-6876

Tony Boualoy

The Ohio State university

Jung Kim

The Ohio State university

Yonggyu Lee

The Ohio State university

Natalia Vanegas

The Ohio State University https://orcid.org/0000-0001-5135-1714

Doug Gouchoe

The Ohio State university

Lorena Rosas

The Ohio State University https://orcid.org/0009-0005-9054-3045

Xi Wang

The Ohio State university

Yuke Hou

The Ohio State university

Mahnoor Hamid

The Ohio State university

Quin Ma

The Ohio State university

Brenda F. Reader

The Ohio State University

Sylvester Black

The Ohio State university

Ana Mora

Ohio State University https://orcid.org/0000-0003-1653-8318

Mauricio Rojas

Ohio State University https://orcid.org/0000-0001-7340-4784

Bryan Whitson

The Ohio State University Wexner Medical Center https://orcid.org/0000-0003-0040-3638

Article

Keywords: CD38, Lung transplantation, Ischemia-reperfusion injury, IRI, NAD⁺ metabolism, Cellular senescence, Donor Management, donation after circulatory death, DCD, Endothelial dysfunction

Posted Date: October 21st, 2026

DOI: https://doi.org/10.21203/rs.3.rs-10988445/v1

License: This work is licensed under a Creative Commons Attribution 4.0 International License.
Read Full License

Additional Declarations: There is **NO** Competing Interest.

Abstract

Cellular senescence increases susceptibility to tissue injury and impairs reparative capacity, yet its role in lung transplantation-associated ischemia-reperfusion injury (IRI) and graft dysfunction remains poorly defined. Because senescence-associated signaling is intricately linked to metabolic dysfunction, we investigated the contribution of Cluster of Differentiation 38 (CD38), a key regulator of NAD^+ homeostasis, to senescence-associated lung inflammation and injury. In lungs procured from human donors, CD38 expression increased with donor age and ischemic stress, particularly in donation after circulatory death (DCD) allografts, and was associated with senescence-associated secretory phenotype (SASP) signaling. In a murine hilar clamp lung IRI model, genetic deletion or pharmacologic inhibition of CD38 preserved NAD^+ levels, attenuated SASP-associated inflammatory mediators, reduced histologic lung injury, and improved pulmonary mechanics. Bronchoalveolar lavage fluid and plasma analyses demonstrated that CD38 deletion or inhibition reduced inflammatory cytokines and cellular injury markers. In human umbilical vein endothelial cells cultures, CD38 knockdown attenuated oxidative stress-induced senescence and cellular injury markers, supporting a direct endothelial mechanism. Collectively, these findings position CD38 as a central mediator linking donor aging and ischemic stress to SASP-driven inflammatory injury and suggest that peri-transplant CD38 targeting may mitigate IRI, preserve allograft quality, and expand the donor lung pool.

INTRODUCTION

Lung transplantation remains the only definitive life-extending therapy for patients with end-stage pulmonary disease. However, donor organ availability remains critically limited. In 2023 alone, 3,427 new patients were added to the U.S. lung transplant waitlist, yet only 3,049 lung transplants were performed, resulting in a waitlist mortality rate of 13.3 deaths per 100 patient-years.[1] Only approximately 3 per 1,000 eligible donors die under circumstances compatible with organ donation, and just 20% of donor lungs are ultimately transplanted.[1,2] Many potentially viable lungs are excluded due to concerns regarding ischemic injury, impaired gas exchange, pulmonary edema, or anticipated post-transplant dysfunction related to donor factors such as advanced age and ischemic exposure.[1,3–6] Long-term survival after lung transplantation also continues to lag behind other solid-organ transplants,[7] with only 31.8% of recipients alive at 10 years.[1,8,9] These persistent shortages have driven increased utilization of extended-criteria donor lungs despite their greater susceptibility to ischemic stress and graft dysfunction.[1–3,10,11]

The increasing reliance on extended-criteria donor lungs has heightened interest in the mechanisms that render these grafts more susceptible to injury. Older donor allografts (≥ 55 years) are associated with increased susceptibility to ischemic injury, graft dysfunction, and reduced post-transplant survival, although the biological mechanisms underlying this vulnerability remain incompletely understood.[12,13] UNOS lung transplant survival data (2019–2025, n = 10,872) illustrate the clinical relevance of donor and recipient age: while overall 5-year survival after lung transplantation approaches 60%, survival declines progressively with increasing donor and recipient age, reaching approximately 50% in older donor older/

recipient pairs. (Fig. 1A). With both recipient and donor ages rising in the U.S, improved strategies are needed to prevent or treat PGD, expand the safe use of extended-criteria lungs, and improve longer-term graft function and transplant outcomes.[11,14]

Donation after circulatory death (DCD) donor lungs represent another major source of extended-criteria grafts. Compared with donation after brain death (DBD) donor lungs, DCD grafts are exposed to longer warm ischemia during procurement and implantation, further exacerbating ischemic stress.[10,14–17] This ischemic exposure contributes to ischemia-reperfusion injury (IRI), an unavoidable consequence of organ procurement and implantation that remains a major driver of early graft dysfunction and impaired long-term survival after lung transplantation.[9,18,19] At the tissue level, IRI induces oxidative stress, inflammation, mitochondrial dysfunction, endothelial injury, and metabolic derangements that collectively disrupt the alveolar microenvironment and promote cellular senescence and progressive alveolar injury (Fig. 1B).[13,20–22]

Clinically, the earliest and most severe manifestation of IRI is primary graft dysfunction (PGD), which affects up to one-third of recipients within 72 hours of transplantation and contributes to early mortality, prolonged hospitalization, and post-transplant complications.[16,23,24] PGD is characterized by alveolar injury, vascular permeability, tissue edema, immune cell infiltration, hypoxemia, and can initiate a cascade of inflammation and extracellular matrix deposition that evolves into chronic lung allograft dysfunction (CLAD), resulting in irreversible loss of function.[9,25–27] Since no approved therapy exists to prevent or treat PGD, concern for early graft injury continues to limit utilization of extended-criteria donor lungs.

Cellular senescence provides a compelling biological framework linking donor risk factors to peri-transplant injury and subsequent graft dysfunction. Senescence is a stress-responsive cellular state characterized by stable cell cycle arrest induced by aging, DNA damage, oxidative stress, inflammatory signaling, and tissue injury.[28–30] As senescent cells accumulate in the lung, they release senescence-associated secretory phenotype (SASP) factors that amplify inflammation, promote immune cell infiltration and fibrogenesis, disrupt cellular metabolism, impair repair, increase resistance to apoptosis, and contribute to persistent injury. Progressive senescence-associated NAD^+ depletion further exacerbates oxidative stress, mitochondrial dysfunction, and inflammatory signaling, creating a self-perpetuating cycle of metabolic dysfunction and worsening lung injury (Fig. 1C).[30,31] Transplant-related IRI may exacerbate these pathways, but the mechanisms by which cellular senescence increases donor lung susceptibility to IRI remain incompletely understood.

Given the central role of NAD^+ homeostasis in regulating cellular metabolism, oxidative stress, and inflammatory signaling, increasing attention has focused on cluster of differentiation 38 (CD38), a key regulator of intracellular calcium signaling through the generation of second messengers, including cyclic ADP-ribose (cADPR) and nicotinic acid adenine dinucleotide phosphate (NAADP).[32–35] CD38 hydrolyzes nicotinamide adenine dinucleotide (NAD^+) and catalyzes a base-exchange reaction involving

nicotinic acid and nicotinamide adenine dinucleotide phosphate ($NADP^+$) to generate NAADP, thereby linking NAD+ depletion with calcium-mobilizing second messenger production.[33,36,37] During cellular stress or injury, CD38 expression is upregulated, amplifying NAD^+ consumption and calcium-dependent signaling.[38,39] Elevated levels of cADPR and NAADP promote intracellular Ca^{2+} mobilization from distinct cellular stores, contributing to reactive oxygen species (ROS) production, oxidative stress, and a proinflammatory cellular phenotype that may promote acute lung injury and early allograft dysfunction.[32,38,39] NAD^+ depletion further impairs sirtuin (SIRT)-dependent signaling, disrupts redox balance, and promotes mitochondrial dysfunction (Fig. 1D).[32,37,40] Together, the CD38/NAD^+/cADPR/NAADP/Ca^{2+} axis links metabolic dysfunction with calcium-driven inflammatory signaling, providing a plausible mechanism by which donor aging and ischemic stress may promote cellular senescence and increase vulnerability to IRI.[41]

Although CD38 expression increases with aging and inflammation across multiple tissues, its contribution to donor lung injury remains poorly defined. Given its central role in regulating NAD^+ homeostasis and calcium-driven inflammatory signaling, CD38 may represent a mechanistic link between donor risk factors, cellular senescence, and susceptibility to IRI. Because the extent to which CD38 contributes to senescence-associated inflammatory injury in deceased donor lungs remains unclear, we examined the role of CD38 in lung transplantation-related IRI using human donor lung tissue and a complementary murine hilar clamp model of lung IRI. Here, we demonstrate that CD38 expression increases with donor age, warm ischemia, and cellular senescence, accompanied by NAD^+ depletion and enhanced inflammatory signaling. We further show that genetic deletion or pharmacologic inhibition of CD38 preserves NAD^+ homeostasis and attenuates lung injury. Together, these findings identify CD38 as a modifiable mediator of age- and injury-associated cellular senescence and suggest that targeting CD38 may preserve donor lung quality and support broader use of extended-criteria lungs during lung transplantation, making this life saving therapy more accessible for all.

RESULTS

CD38 expression and senescence-associated marker burden increase with age and ischemic stress in deceased donor lungs

We first examined the relationship between donor and recipient age and post-lung transplant survival to assess the clinical impact of age on survival outcomes, in a national cohort. Survival differed significantly across donor-recipient age strata by log-rank test ($p < 0.0001$), with the lowest survival observed among older recipients receiving lungs from older donors (Fig. 1A). These findings support the clinical relevance of donor and recipient age as factors associated with impaired long-term survival, raising the possibility that age-associated biological processes may contribute to graft vulnerability. Given the clinical association observed between donor and recipient age and post-transplant survival, we sought to determine whether these findings translated into age- and ischemic stress associated differences in CD38 expression. CD38 expression increased progressively with both donor age and

ischemic stress. Compared with young DBD lungs, CD38 expression was modestly increased in older DBD donors and in younger DCD donors, while the highest expression was observed in older DCD allografts, suggesting additive effects of donor aging and ischemic stress (Fig. 2A). Immunohistochemical analysis localized CD38 expression to the alveolar, vascular, and airway epithelium and demonstrated progressively increased staining intensity and abundance of CD38-positive cells across donor age and ischemic stress groups, with the most extensive staining observed in older DCD lungs (Fig. 2B). Together, these findings demonstrate that CD38 expression increases in donor allografts exposed to aging and ischemic stress, identifying CD38 as a candidate mediator linking donor risk factors to cellular senescence and graft injury.

Given the marked increase in CD38 expression observed in older DCD lungs, we next sought to determine whether elevated CD38 expression was accompanied by evidence of cellular senescence, SASP signaling, and endothelial dysfunction. To focus on the donor population exhibiting the greatest CD38 burden and ischemic stress exposure, subsequent analyses were performed in DCD donor lungs stratified by age. Western blot analysis demonstrated increased expression of CD38, senescence-associated markers, and ET-1 a marker of endothelial dysfunction implicated in ischemia-reperfusion injury and primary graft dysfunction, in older compared with younger DCD donors as supported by densitometric analysis (p16, $p = 0.0389$; p53, $p = 0.0477$; p21, $p = 0.0294$; ET-1, $p = 0.00040$; CD38, $p = 0.026$) (Fig. 2C). Consistent with these findings, ELISA-based analyses demonstrated higher ET-1, IL-1β, and TNF in older compared with younger DCD donor lungs (ET-1, $p = 0.0026$; IL-1β, $p = 0.0011$; TNF-α, $p = 0.0416$) **(Fig. 2D)**, while enzymatic activity assays demonstrated increased CD38 activity (CD38 activity, $p = 0.0489$) (Fig. 2E).

Since CD38 is a NADase, we next assessed NAD^+/NADH ratios in human donor lung tissue. Older donor lungs demonstrated significantly lower NAD^+/NADH ratios than those of younger donors in both DBD and DCD groups (DBD: $p = 0.0002$; DCD: $p < 0.0001$) **(Fig. 2F)**. These reductions coincided with observed increases in CD38 expression, senescence-associated markers, and inflammatory mediators in older and DCD lungs. Collectively, these data link donor age and ischemic stress to CD38 upregulation, NAD^+ depletion, and senescence-associated inflammatory signaling.

Single Cell Profiling of Donor Lungs by Age and Donor Type

Single-cell RNA sequencing (scRNA-seq) was performed to characterize senescence-associated transcriptional programs according to donor age and donor type. Cell-type annotation identified distinct epithelial, immune, mesenchymal, and endothelial populations, with cellular composition varying across donor groups (Fig. 3A). Epithelial representation declined from 40.5% in younger DBD lungs to 29.4% in older DBD, 27.1% in younger DCD, and 18.1% in older DCD lungs. Conversely, endothelial representation increased across these groups (9.9%, 14.6%, 17.1%, and 25.2%, respectively), while mesenchymal representation was lowest in younger DBD lungs (12.2%) and highest in older DCD lungs (21.0%).

These compositional changes suggest that increasing age and DCD status are associated with reduced epithelial representation and relative expansion of the endothelial and mesenchymal compartments. This pattern is consistent with the vulnerability of the pulmonary epithelium to ischemia-reperfusion injury and the impaired regenerative capacity of senescent alveolar progenitor cells. The relative enrichment of endothelial cells and fibroblast populations, including inflammatory and CTHRC1$^+$ fibroblasts, may further contribute to vascular dysfunction, senescence-associated signaling, and profibrotic repair. Because scRNA-seq cell proportions are compositional and constrained to sum to unity, these differences reflect relative rather than absolute abundance. Nevertheless, the shift from epithelial toward endothelial and mesenchymal populations suggests a cellular environment that may promote persistent inflammatory signaling while limiting epithelial recovery.

SenMayo scores were subsequently evaluated within the endothelial, mesenchymal, and epithelial compartments (Fig. 3B) and projected onto the full UMAP embedding to visualize the distribution of senescence-associated transcriptional activity across the dataset (Fig. 3C). Scores were significantly higher in DCD than in DBD lungs across all three compartments.

This increase extended to every pulmonary subpopulation examined (Fig. 3D). Compared with DBD lungs, DCD lungs exhibited significantly higher SenMayo scores in aerocyte capillary (aCap), general capillary (gCap), systemic venous, and venular endothelial cells; adventitial, alveolar, inflammatory, and CTHRC1$^+$ fibroblasts; and alveolar type 1 (AT-1), alveolar type 2 (AT-2), basal, and ciliated epithelial cells. In contrast, scores did not differ significantly by age within either donor group, suggesting that DCD status was more strongly associated with senescence-related transcriptional activity than donor age in this cohort.

Together, these findings reveal widespread senescence-associated transcriptional activity across the pulmonary epithelial, mesenchymal, and endothelial compartments of DCD lungs. In conjunction with the relative expansion of endothelial and mesenchymal populations, these results highlight the pulmonary endothelium as a potential site of CD38-mediated senescence in the donor allograft.

Spatial profiling of airway cellular composition in donor lungs

To understand the spatial context of donor lung tissue, high-resolution Xenium in situ imaging was used to map cellular organization and gene expression within donor airways (Fig. 3E). Airways from both DCD and DBD lungs exhibited a well-defined pseudostratified epithelial layer marked by ATP1A1 and E-cadherin, with dense DAPI-labeled nuclei. The underlying stromal compartment contained α-SMA$^+$ smooth muscle bundles, vimentin-expressing stromal cells, and CD45$^+$ leukocytes, while 18S ribosomal RNA signal delineated transcriptionally active regions.

Senescence-associated transcripts were then mapped relative to the KRT5$^+$/KRT17$^+$ basal epithelial compartment. CDKN1A and CDKN2A, encoding p21 and p16, respectively, were more abundant within the airway epithelium of DCD lungs than in DBD lungs. This spatial pattern corroborated the elevated

senescence scores observed in basal epithelial cells by scRNA-seq (Fig. 3D). BIRC3 expression was also more prominent than pro-apoptotic BAX expression in DCD airways, consistent with the apoptosis-resistant phenotype associated with cellular senescence. In addition, CTHRC1 transcripts localized to the subepithelial stromal compartment, corresponding anatomically to the CTHRC1^{+} fibroblast population identified by single-cell profiling.

Together, these spatial data localize senescence-associated expression to the airway epithelium and adjacent stroma of DCD donor lungs. CDKN1A and CDKN2A expression was concentrated within the KRT5^{+}/KRT17^{+} basal epithelial population, whereas profibrotic CTHRC1 expression localized to the underlying stroma. Detection of these transcripts within intact tissue architecture supports the single-cell findings and reduces the likelihood that the observed transcriptional programs resulted solely from tissue dissociation.

Genetic and pharmacologic inhibition of CD38 mitigates IRI in mice

To determine whether CD38 directly contributes to lung IRI, we employed complementary genetic and pharmacologic approaches in a murine hilar clamp model. Wild-type (WT) and CD38 knockout (CD38$^{-/-}$) mice underwent one hour of left hilar ischemia followed by 24 hours of reperfusion using a well-established hilar clamp model (Fig. 4A).[42] Experimental groups included WT sham, CD38$^{-/-}$, WT sham treated with 78c, WT IRI, CD38$^{-/-}$ IRI, and WT treated with 78c mice. Pharmacologic inhibition was achieved using 78c, a well-characterized, selective small-molecule inhibitor of CD38 that has previously been shown to preserve NAD^{+} homeostasis and attenuate ischemia-reperfusion injury in preclinical models.[43,44]

Both CD38$^{-/-}$ mice and 78c treatment conferred preserved pulmonary function following IRI. Inspiratory capacity was significantly reduced following WT IRI compared with WT sham controls ($p = 0.0336$), and was preserved in both CD38KO IRI ($p = 0.0084$) and WT IRI + 78c lungs ($p = 0.0340$) relative to WT IRI. Static compliance was significantly improved in CD38KO IRI lungs compared with WT IRI ($p = 0.0012$), and in WT IRI + 78c models ($p = 0.0103$). Pressure-volume loop area was likewise improved in both CD38KO IRI ($p = 0.0286$) and WT IRI + 78c lungs ($p = 0.0205$) relative to WT IRI controls, consistent with preserved ventilatory mechanics following CD38 deletion or inhibition (Fig. 4B).

Bronchoalveolar lavage (BAL) cytospin preparations demonstrated marked inflammatory cellular infiltration following WT IRI compared with sham controls (Fig. 4C). Both CD38 deletion and pharmacologic inhibition with 78c reduced inflammatory cell infiltration following IRI. BAL fluid analysis similarly demonstrated significantly increased levels of lactate dehydrogenase (LDH), hyaluronic acid (HA), and IL-6 following WT IRI, consistent with increased lung injury and inflammatory signaling. Compared with WT IRI controls, CD38$^{-/-}$ and WT IRI + 78c groups demonstrated significantly reduced LDH (both $p < 0.0001$), HA (both $p < 0.0001$), and IL-6 levels (both $p < 0.0001$) (Fig. 4D).

Histologic evaluation demonstrated substantial architectural disruption following WT IRI, characterized by diffuse alveolar septal thickening, interstitial and alveolar edema, inflammatory cellular infiltration, and loss of normal alveolar architecture. In contrast, both $CD38^{-/-}$ and WT IRI + 78c lungs demonstrated preservation of alveolar structure with reduced septal thickening, diminished inflammatory infiltration, and decreased edema compared with WT IRI lungs, consistent with attenuation of IRI-associated tissue injury (Fig. 4E).

Lung tissue analysis revealed increased p16, p53, and CD38 expression following IRI relative to WT sham (p16, $p = 0.0195$; p53, $p = 0.0245$; CD38, $p = 0.0044$). CD38 deletion reduced p16 ($p = 0.0226$), p21 ($p = 0.0397$), p53 ($p = 0.0187$), and CD38 ($p < 0.0001$) expression relative to WT mice subjected to IRI. Treatment with 78c also significantly reduced CD38 expression relative to WT IRI ($p = 0.0188$) but did not significantly alter p16, p21, or p53 expression, consistent with inhibition of CD38 enzymatic activity rather than of CD38 protein abundance (Fig. 4F).

Plasma cytokine analysis demonstrated significantly reduced TNF-α, IL-1β, and IL-18 in CD38KO IRI and WT IRI + 78c groups compared with WT mice subjected to IRI (all $p < 0.01$), along with reduced circulating hyaluronic acid ($p < 0.0001$) (Fig. 4G). To determine whether these effects corresponded to suppression of CD38 catalytic function, CD38 enzymatic activity was measured directly. CD38 activity was markedly increased following WT IRI relative to WT sham ($p < 0.0001$) and was significantly reduced by both 78c treatment and genetic deletion of CD38 (both $p < 0.0001$) (Fig. 4H), confirming that the observed protection was accompanied by suppression of CD38 enzymatic activity.

Natural flavonoid inhibitors of CD38 attenuate senescence & preserve lung function after IRI

Building on these findings, we next evaluated whether naturally occurring flavonoids with known CD38-inhibitory and senescence-modulating properties could similarly attenuate lung IRI. Quercetin has been shown to directly inhibit CD38 enzymatic activity and preserve intracellular NAD^+ homeostasis, whereas fisetin has demonstrated potent senolytic and anti-inflammatory effects and has been identified among flavonoids with reported CD38-inhibitory activity.[45–48] Accordingly, we assessed the effects of quercetin and fisetin in the murine hilar clamp model of lung IRI. WT mice were treated with quercetin (50 mg/kg) or fisetin (100 mg/kg) prior to ischemia and then subjected to one hour of left-lung ischemia followed by 24 hours of reperfusion (Fig. 5A). Flavonoid treatment preserved pulmonary function following IRI. Inspiratory capacity was higher in both IRI+quercetin ($p = 0.0220$) and IRI+fisetin lungs ($p = 0.0120$) relative to untreated WT IRI controls, as was static compliance (quercetin, $p = 0.0004$; fisetin, $p = 0.0008$). Pressure-volume loop area was improved in IRI+quercetin lungs ($p = 0.0042$) compared with WT mice subjected IRI (Fig. 5B). Histologic assessment demonstrated attenuation of tissue injury in flavonoid-treated animals. Untreated IRI lungs exhibited diffuse alveolar edema, architectural disruption, and inflammatory infiltration, whereas quercetin and fisetin-treated lungs preserved alveolar architecture with reduced edema and inflammatory cell infiltration (Fig. 5C).

Flavonoid-treated animals demonstrated reduced plasma markers of injury and inflammation, with marked reductions in ET-1 ($p < 0.0001$) and IL-18 ($p = 0.0001$), alongside decreased IL-1β ($p = 0.0004$), TNF-α ($p = 0.0211$), and LDH ($p = 0.0092$) compared with untreated IRI controls (Fig. 5D). To determine whether the protective effects of flavonoid treatment were accompanied by modulation of CD38-associated senescence and injury pathways, protein expression was assessed in lung tissue following IRI. Both quercetin and fisetin reduced CD38 expression ($p = 0.0008$ and $p < 0.0001$, respectively) and attenuated markers of cellular senescence, including p53 ($p = 0.0215$ and $p = 0.0131$, respectively) and p21 ($p = 0.0036$ and $p = 0.0127$, respectively), compared with untreated IRI controls. Flavonoid treatment was also associated with reduced expression of ET-1, a marker of endothelial dysfunction ($p = 0.0037$ and $p = 0.0350$, respectively), and HMGB1, a damage-associated molecular pattern released during cellular injury and sterile inflammation ($p = 0.0258$ and $p = 0.0042$, respectively) (Fig. 5E-F). Together, these findings demonstrate that quercetin and fisetin recapitulate the protective phenotype observed with genetic and pharmacologic CD38 inhibition, attenuating senescence-associated signaling, endothelial dysfunction, and tissue injury following lung IRI.

CD38-mediated senescence signaling and injury are recapitulated in human endothelial cells during hypoxia-reoxygenation

Given the prominent endothelial injury that characterizes lung IRI and PGD, as well as the increased vascular CD38 and ET-1 expression observed in donor lungs, we next evaluated the contribution of CD38 to endothelial dysfunction. Human umbilical vein endothelial cells (HUVECs) were subjected to hypoxia-reoxygenation (H/R) injury and CD38 expression was suppressed using siRNA-mediated silencing (Fig. 6A). Efficient CD38 knockdown was confirmed, with a marked reduction in CD38 protein expression compared with control cells (Fig. 6B). CD38 inhibition improved endothelial cell survival following H/R injury. Both siRNA-mediated CD38 knockdown and 78c treatment improved endothelial survival following H/R injury, with increased cell viability ($p < 0.0001$) and reduced LDH release ($p < 0.0001$) compared with untreated controls (Fig. 6C). Consistent with induction of a senescent phenotype, H/R injury significantly increased expression of CD38 ($p < 0.0001$), p16 ($p = 0.0008$), p21 ($p = 0.0007$), and p53 ($p = 0.0031$), while also increasing senescence-associated β-galactosidase (SA-β-gal) activity, a widely used marker of senescent cell burden (Fig. 6D). These changes were attenuated by both siRNA-mediated CD38 knockdown and pharmacologic inhibition with 78c, supporting a role for CD38 in mediating endothelial senescence signaling in response to hypoxic stress. Extending these findings, HUVECs were then treated with either quercetin or fisetin following H/R injury to determine whether flavonoid-mediated CD38 inhibition similarly attenuates endothelial senescence. Flavonoid treatment attenuated the senescent phenotype induced by H/R injury, reducing expression of the senescence-associated markers p53 (fisetin: $p = 0.0004$; quercetin: $p = 0.0138$), p21 (fisetin: $p = 0.0008$; quercetin: $p = 0.0094$), and p16 (fisetin: $p = 0.0481$; quercetin: $p = 0.0005$) compared with untreated H/R controls (Fig. 6E). Notably, quercetin and fisetin produced a pattern of senescence marker suppression similar to that observed following siRNA-mediated CD38 silencing, supporting a role for CD38 in regulating endothelial senescence during hypoxia-reoxygenation injury. Together, these findings demonstrate that CD38-mediated senescence

signaling is recapitulated in human endothelial cells and is attenuated by suppression of CD38-driven signaling.

COMMENTS

Cellular senescence has emerged as a fundamental determinant of tissue vulnerability during aging and injury, yet its contribution to donor lung quality and transplant outcomes remains incompletely understood. In this study, we identify CD38 as a central regulator linking donor age, ischemic stress, and senescence-associated injury in the lung. Elevated CD38 expression was associated with advanced donor age, donation after circulatory death (DCD), prolonged ischemic exposure, and increased expression of senescence-associated markers in human donor lungs. Across complementary human, murine, and endothelial cell models, inhibition of CD38 through genetic deletion, siRNA-mediated silencing, pharmacologic blockade with 78c, or treatment with the naturally occurring flavonoids quercetin and fisetin consistently attenuated senescence-associated signaling, reduced inflammatory and injury-related mediators, and improved functional outcomes. Collectively, these findings identify CD38 as a conserved and targetable mediator of donor lung injury and support a mechanistic role for CD38 in linking aging and ischemic stress to cellular senescence and graft dysfunction.

Although CD38 has well-established roles in NAD^+ metabolism and inflammatory signaling, its contribution to lung transplant-related injury has remained poorly defined. Here, we demonstrate that increased CD38 expression is consistently associated with senescence-associated signaling across human donor lungs, murine ischemia-reperfusion injury (IRI), and human endothelial cells subjected to hypoxia-reoxygenation. These findings extend prior observations linking CD38 to aging and chronic inflammatory disease and suggest that CD38 serves as an important metabolic regulator of stress-induced senescence in the transplant setting.[37,38] Rather than representing a passive consequence of aging or ischemic injury, our data support a model in which senescence actively contributes to donor lung vulnerability and graft dysfunction. In this framework, CD38 functions as a critical molecular node linking metabolic stress to inflammatory and senescence-associated responses that impair tissue resilience.

A central observation of this study is the association between increased CD38 expression and reduced NAD^+ availability in donor lungs exposed to aging and ischemic stress. NAD^+ plays a fundamental role in regulating mitochondrial function, redox homeostasis, DNA repair, and cellular stress responses.[38,49–51] Progressive NAD^+ decline is increasingly recognized as a hallmark of biological aging, and CD38 has emerged as one of its principal consumers.[37,52] Our findings extend these concepts to lung transplantation and suggest that ischemic stress may accelerate similar metabolic derangements in donor organs. The observation that both genetic and pharmacologic CD38 inhibition attenuated injury while suppressing senescence-associated signaling supports the concept that preservation of NAD^+ homeostasis represents a mechanistically important component of donor lung protection. Together, these findings place metabolic dysfunction at the center of donor lung susceptibility and suggest that

interventions targeting NAD^+ consumption may have therapeutic relevance during donor management and organ preservation.

Notably, the greatest CD38 expression and senescence burden were observed in older DCD donor lungs, suggesting that donor age and ischemic exposure converge on common metabolic and inflammatory pathways. This finding is particularly relevant given the increasing reliance on extended-criteria donors to address persistent organ shortages.[2,10,11] Although DCD transplantation has achieved outcomes comparable to conventional donation in carefully selected recipients,[14,53] concern regarding warm ischemic injury continues to limit broader utilization and contributes to ongoing donor lung discard. Our findings raise the possibility that CD38-mediated metabolic dysfunction contributes to this vulnerability and may represent a targetable mechanism for improving recovery and utilization of DCD donor lungs. Identification of biologic pathways that underlie donor organ quality may become increasingly important as transplant programs continue to expand acceptance criteria for older and higher-risk donors.

The endothelial studies further support a direct role for CD38 in regulating cellular responses to ischemic stress. Endothelial dysfunction is increasingly recognized as an important component of both IRI and PGD. ET-1, a potent endothelial-derived vasoconstrictor, is rapidly upregulated following ischemia-reperfusion injury and contributes to microvascular dysfunction, inflammatory cell recruitment, and impaired tissue perfusion.[54–57] Aging has also been associated with increased endothelial ET-1 expression and release, creating a pro-inflammatory and vasoconstrictive vascular phenotype.[58,59] Consistent with these observations, ET-1 expression was increased in aged and ischemically stressed donor lungs and was attenuated following genetic, pharmacologic, and flavonoid-mediated CD38 inhibition. Furthermore, CD38 silencing in human endothelial cells reduced SAS and improved cellular resilience following hypoxia-reoxygenation injury. These findings suggest that endothelial cells may represent an important cellular target through which CD38 contributes to graft injury and provide mechanistic support for the broader observations observed in donor lungs and experimental IRI.

From a translational perspective, these findings highlight CD38 as an attractive therapeutic target for donor lung preservation. Modulation of CD38 activity could potentially be incorporated into donor management strategies, organ preservation solutions, or *ex vivo* lung perfusion (EVLP) protocols to reduce metabolic stress and limit senescence-associated injury prior to implantation. The protective effects observed with both the selective CD38 inhibitor 78c and naturally occurring flavonoids suggest multiple potential avenues for therapeutic development. While additional work will be required to define optimal dosing, timing, and delivery strategies, transient inhibition of CD38 during donor preparation may represent a feasible approach to preserve graft quality, improve resistance to ischemic injury, and expand the transplantable donor organ pool.

Several limitations warrant consideration. Although 78c is widely regarded as a selective CD38 inhibitor, off-target effects cannot be completely excluded. However, the concordant protective effects observed following genetic deletion, siRNA-mediated silencing, selective pharmacologic inhibition, and treatment with multiple flavonoids support a central role for CD38 in mediating the observed phenotype. Similarly,

quercetin and fisetin possess pleiotropic antioxidant, anti-inflammatory, and senolytic properties that likely contribute to their protective effects independent of CD38 inhibition. Findings from human donor tissue remain associative and may be influenced by unmeasured donor, procurement, and peri-transplant variables. Additionally, endothelial experiments were performed using HUVECs, which may not fully recapitulate the biology of pulmonary microvascular endothelial cells. Validation in primary human lung endothelial cells, *ex vivo* donor lung models, and clinically relevant EVLP platforms will further strengthen mechanistic understanding and translational applicability. Furthermore, the temporal relationships among CD38 activation, NAD^+ depletion, senescence induction, and inflammatory signaling remain incompletely defined. Future studies incorporating longitudinal sampling and mechanistic interrogation of upstream regulators of CD38 expression will help clarify the sequence of events that drive graft injury.

In conclusion, CD38 expression increases with donor age and ischemic stress and is associated with NAD^+ depletion, cellular senescence, and lung injury. Genetic, pharmacologic, and flavonoid-mediated inhibition of CD38 consistently attenuated senescence-associated signaling and improved functional outcomes across human donor tissues, murine IRI, and human endothelial cell models. These findings identify CD38 as a mechanistically important mediator of donor lung vulnerability and support targeting CD38 as a potential strategy to improve donor lung preservation, expand utilization of extended-criteria organs, and enhance transplant outcomes.

METHODS

Animals

All in vivo experiments used C57BL/6J WT mice (The Jackson Laboratory, Bar Harbor, ME) weighing 20–30 g and aged 8–12 weeks. CD38 knockout ($CD38^{-/-}$) mice on a C57BL/6J background were obtained from The Jackson Laboratory. Absence of CD38 protein expression in $CD38^{-/-}$ mice was confirmed by PCR genotyping immunoblotting prior to experimental use. All animals were housed under standard conditions (humidity: 45%-70%, temperature: 21°C ± 3°C, 12-hour light-dark cycle) and provided ad libitum access to water and standard chow. Animal experiments were carried out with the approval of The Ohio State University Institutional Animal Care and Use Committee (IACUC protocol #2023A00000071). All procedures were performed in strict accordance with the National Institutes of Health Guide for the Care and Use of Laboratory Animals (NIH Publications No. 8023, revised 2011, National Academies Press).

Lung Ischemia-Reperfusion Injury Model

For IRI experiments, $CD38^{-/-}$ and WT mice were randomly assigned to treatment groups. Protocols for the murine left hilar clamp model have been described in detail.[57,60] Briefly, mice were anesthetized with inhaled isoflurane (2% in oxygen), intubated, and a surgical plane of anesthesia was established. A left anterolateral thoracotomy was performed, and the left hilum (pulmonary artery, vein, and bronchus) was occluded *en bloc* using a small atraumatic vascular clamp for 1 hour to induce warm ischemia. Sham-operated animals underwent identical thoracotomy without hilar occlusion. Pharmacologic treatments

were administered immediately prior to reperfusion unless otherwise specified. For CD38 inhibition studies, WT mice received 78c (15 mg/kg) via intravenous injection. In separate experimental arms, WT mice were treated with quercetin (50 mg/kg) or fisetin (100 mg/kg) by oral gavage once daily for 7 days prior to ischemia induction. After 60 minutes, the clamp was removed to initiate reperfusion. Recruitment maneuvers were performed by increasing positive end-expiratory pressure to 6 cmH_2O, and the thoracotomy incision was closed in two layers. Animals recovered with standard postoperative analgesia and were maintained for 24 hours following reperfusion. At the time of euthanasia, animals were re-anesthetized, the trachea was surgically exposed, and a tracheal cannula was inserted for pulmonary mechanics assessment as described below. Following completion of lung function measurements, blood was collected from the inferior vena cava via midline laparotomy. Animals were euthanized by transection of the inferior vena cava, and the thoracic cavity was exposed.

Bronchoalveolar lavage (BAL) was performed. The right and left auricles were incised, and the lungs were flushed through the pulmonary artery using prechilled phosphate-buffered saline (PBS) (Gibco, Waltham, MA). The heart-lung block was then removed. The left lung was divided into two portions: the upper region was snap-frozen in liquid nitrogen for molecular analyses, and the lower region was fixed for histologic evaluation. Blood, BAL fluid, and tissue samples were processed for downstream biochemical and molecular analyses as described below.

Lung Function Assessment

Pulmonary mechanics were measured 24 hours after reperfusion using the flexiVent system (SCIREQ). The flexiVent system was calibrated according to manufacturer specifications prior to each experiment. Mice were anesthetized, tracheostomized, paralyzed (Rocuronium, 1 mg/kg), and mechanically ventilated. Following two standardized deep inflation maneuvers to normalize lung volume history, respiratory mechanics were measured using broadband forced oscillation perturbations. Parameters recorded included inspiratory capacity (IC), static compliance (Cstat) and pressure-volume loop (Area). For each animal, at least three measurements were recorded and averaged. Data were analyzed using flexiWare software (SCIREQ) and exported for statistical analysis.

Cell Culture

HUVECs were obtained from American Type Culture Collection (ATCC; Manassas, VA) and cultured in F-12K medium supplemented with 10% fetal bovine serum following standard ATCC culture conditions. Cells were cultured at 37°C in a humidified incubator containing 5% CO_2. Medium was refreshed 12–24 hours before experimental manipulation. Only cultures exhibiting typical endothelial cobblestone morphology were used for downstream analyses. All experiments were performed using biological replicates derived from independent passages.

siRNA-Mediated CD38 Knockdown

CD38 knockdown (KD) was achieved by transfection of CD38 siRNA (Thermo Fisher Scientific; catalog no. 197819) using Lipofectamine RNAiMAX transfection reagent (Thermo Fisher Scientific). HUVECs

were seeded to achieve 50–60% confluence at the time of transfection. CD38-targeting siRNA or scrambled control siRNA (Thermo Fisher Silencer Negative Control 1) was diluted in Opti-MEM medium and combined with RNAiMAX reagent. The mixtures were incubated for 20 minutes at room temperature to allow formation of siRNA-lipid complexes.

The complexes were added to cells maintained in Opti-MEM medium. After 12 hours of transfection, the medium was replaced with complete growth medium, and cells were allowed to recover for an additional 12 hours before experimental manipulation. Knockdown efficiency was confirmed by Western blot analysis, demonstrating reduction in CD38 protein expression compared with scrambled control treated cells. All siRNA experiments were performed in biological triplicate using independent cell passages.

Hypoxia-Reoxygenation

To model IRI-like stress *in vitro*, HUVECs were subjected to hypoxia-reoxygenation (H/R). For hypoxia exposure, culture plates were transferred to a modular hypoxia chamber equilibrated to 1% O_2, 5% CO_2, and balanced N_2 at 37°C for 3 hours. Hypoxic conditions were confirmed using an in-line oxygen sensor. Following hypoxia, cells were returned to normoxic conditions (21% O_2, 5% CO_2) for 3 hours to allow reoxygenation. Control cells were maintained under normoxic conditions for the same duration. CD38 activity was modulated using complementary genetic and pharmacologic approaches. For genetic knockdown, HUVECs were transfected with siRNA targeting CD38 or a non-targeting control siRNA using a lipid-based transfection reagent according to the manufacturer's instructions. Knockdown efficiency was confirmed by immunoblotting prior to H/R experiments. For pharmacologic inhibition, cells were treated with 78c at the indicated concentrations prior to hypoxia and maintained throughout both hypoxic and reoxygenation phases. In parallel experiments, cells were treated with the natural flavonoids quercetin or fisetin and maintained under identical H/R conditions. Cells were harvested immediately following reoxygenation for downstream molecular, biochemical, and morphologic analyses.

Western Blot Analysis

Lung tissue was homogenized in radioimmunoprecipitation assay (RIPA) lysis buffer (Millipore, Temecula, CA) supplemented with 1× protease/phosphatase inhibitor cocktail (Cell Signaling Technology, Beverly, MA). Cultured endothelial cells were lysed in the same buffer under identical conditions. Lysates were clarified by centrifugation, and protein concentration was determined using a standard colorimetric assay. Equal amounts of lysate protein were electrophoresed on 6% to 12% sodium dodecyl sulfate polyacrylamide gel electrophoresis (SDS-PAGE) gels and transferred onto PVDF membranes. Nonspecific binding was blocked by incubation in Tris-buffered saline containing 0.1% Tween-20 supplemented with 5% nonfat dry milk for 3 hours at room temperature. Membranes were incubated overnight at 4°C with primary antibodies against CD38, p16, p21, p53, endothelin-1 (ET-1), and senescence-associated β-galactosidase (SA-β-gal). Membranes were then incubated with horseradish peroxidase-conjugated secondary antibodies (Jackson ImmunoResearch Laboratories, West Grove, PA) for 1 hour at room temperature. Protein levels were detected using Western Lightning Plus-ECL (PerkinElmer, Waltham, MA). β-actin (Sigma-Aldrich, St. Louis, MO) was used as a loading control.

Quantitative densitometric analysis was performed using ImageJ software (NIH), and target protein expression was normalized to β-actin.

Enzyme-Linked Immunosorbent Assay (ELISA)

Tissue homogenates were collected from the lungs, and bronchoalveolar lavage (BAL) fluid and plasma were obtained as described above. The levels of hyaluronic acid (HA), tumor necrosis factor alpha (TNF-α), and interleukin-1β (IL-1β) were measured by enzyme-linked immunosorbent assay according to the manufacturer's instructions (R&D Systems, Minneapolis, MN). Absorbance was measured using a POLARstar Omega multi-mode microplate reader (BMG LABTECH, Ortenberg, Germany).

CD38 Enzymatic Activity Assay

CD38 NAD(P) + ase activity was measured using fluorescence detection as previously described. The NAD+ analog nicotinamide 1,N^6-ethenoadenine dinucleotide (ε-NAD) was used as substrate for NAD(P)ase activity measurements. For each assay, cell or lung tissue lysate containing 50 µg of total protein was added to a 100 µL reaction mixture containing 200 µM ε-NAD. Reactions were monitored for the conversion of ε-NAD to the fluorescent product ε-ADP-ribose (ε-ADPR). Fluorescence intensity was measured at an excitation wavelength of 300 nm and an emission wavelength of 410 nm using a POLARstar Omega multi-mode microplate reader (BMG LABTECH, Ortenberg, Germany). Enzymatic activity was calculated as the rate of substrate conversion normalized to total protein concentration. Background fluorescence from samples lacking substrate was subtracted from all measurements. Where indicated, samples treated with the selective CD38 inhibitor 78c served as assay specificity controls.

NAD^+ Quantification

Intracellular NAD^+ levels were quantified in lung tissue lysates and cultured endothelial cells using a colorimetric/fluorometric NAD^+ quantification assay. Briefly, tissue samples were homogenized in NAD^+ extraction buffer and subjected to heat extraction to release intracellular NAD^+. Cell lysates were prepared under identical conditions. Extracts were clarified by centrifugation; supernatants were used for analysis. NAD^+ levels were determined by enzymatic cycling reaction, and absorbance/ fluorescence was measured using a POLARstar Omega multi-mode microplate reader (BMG LABTECH, Ortenberg, Germany) at the recommended wavelength. NAD^+ concentrations were calculated from standard curves generated using known concentrations of NAD^+ and normalized to total protein content.

Lactate Dehydrogenase (LDH) Assay

Lactate dehydrogenase (LDH) release was measured in bronchoalveolar lavage (BAL) fluid and plasma using the LDH cytotoxicity detection assay kit (Clontech Laboratories, Mountain View, CA) according to the manufacturer's instructions. The optical density values were analyzed at 492 nm and normalized relative to plate reference absorbance at 620 nm and background LDH in control wells.

β-Galactosidase Assay

Cellular senescence was assessed using a senescence-associated β-galactosidase (SA-β-gal) staining assay. Following experimental treatment, HUVECs were fixed and incubated with β-galactosidase staining solution according to the manufacturer's protocol. Staining was performed at 37°C under atmospheric CO_2 conditions for the recommended duration. Stained cells were imaged using bright-field microscopy. The percentage of SA-β-gal–positive cells were quantified from randomly selected fields using ImageJ (NIH).

Bronchoalveolar Lavage (BAL) Collection and Processing

Bronchoalveolar lavage (BAL) was performed 24 hours after reperfusion immediately following physiologic assessment. Following tracheal cannulation, the lungs were lavaged with 1.6 mL of sterile, cold PBS instilled in 2 × 0.8 mL aliquots and gently withdrawn after each instillation. Recovered BAL fluid was centrifuged at 800 x g for 10 minutes at 4°C to separate cellular and acellular fractions. The supernatant was collected and stored at − 80°C for cytokine, LDH, and hyaluronic acid measurements. Cell pellets were resuspended in PBS for total and differential cell counts as indicated. Total cell counts were determined using automated cell counter, and differential cell counts were assessed on Cytospin preparations stained with Diff-Quik (Electron Microscopy Sciences, Hatfield, PA, USA).

Histology

Histological samples were stored in 10% neutral-buffered formalin and transferred to ethanol for paraffin embedding. Five-micrometer sections were cut and processed. Hematoxylin–eosin (H&E) staining was performed using standard methods to evaluate lung architecture and tissue injury.

Human Donor Lung Tissue

Human donor lung tissue samples were obtained from DCD and DBD donors through the Comprehensive Transplant Center (CTC) Human Tissue Biorepository at The Ohio State University Wexner Medical Center. Tissue was procured at the time of organ recovery from lungs deemed unsuitable for transplantation. All tissue acquisition and use were approved by the Institutional Review Board of The Ohio State University (IRB study ID 2021H0180). Written informed consent and research authorization were obtained in accordance with institutional and federal guidelines. The CTC Human Tissue Biorepository operates in compliance with NCI and ISBER Best Practices for Repositories. Donor demographic and clinical data, including age and donor type (DCD vs. DBD), were collected in a de-identified manner and linked to tissue samples for downstream analysis.

scRNA-Sequencing using Fixed RNA Profiling (FRP)

Tissue Procurement and FFPE Block Selection. Formalin-fixed paraffin-embedded (FFPE) lung tissue blocks were retrieved from the Comprehensive Transplant Center (CTC) Human Tissue Biorepository at OSU. Total Transplant Care Protocol informed written consent and research authorization form were obtained from all donors in accordance with NCI and ISBER Best Practices for Repositories and was performed by the CTC Human Tissue Biorepository at OSU.

FFPE blocks were selected based on pre-defined quality criteria: fixation time between 12–24 hours in 10% neutral buffered formalin, tissue age no greater than three years from time of archival, ≥ 30% DV200 metric was used to determine the RNA quality and effectively parse samples suitable for NGS from unsuitable samples. Also, hematoxylin and eosin (H&E) staining was used to confirm the tissue integrity, and a pathologist reviewed all sections prior to molecular processing. Serial 10 µm sections were cut using RNase-free microtome blades (Leica, HistoCore BIOCUT) to minimize cross-contamination.

Library preparation and sequencing. FFPE blocks were processed to generate dissociated nuclei suitable for targeted probe based transcript capture according to Demonstrated Protocol CG000632, Rev D (10x genomics).

The FRP chemistry employs RNA probe ligation and barcoding strategies optimized for fragmented, cross linked FFPE RNA, enabling recovery of single cell expression profiles from archival lung tissue. GEM generation and barcoded DNA libraries were prepared using platform integrated reagents according to Chromium Fixed RNA Profiling Reagent Kits for Multiplexed Samples, User Guide CG000527, Rev F (10x genomics) - with a target of 8,000 cells per sample. Library quality was assessed using the Agilent Bioanalyzer High Sensitivity DNA chip and Qubit fluorometer. Pooled libraries were sequenced on an Illumina NovaSeq 6000 sequencer with the following sequencing parameters: depth of 15,000 read pairs per cell, sequencing type Paired-end, dual indexing type, and read lengths of 28 cycles for Read 1, 10 cycles for i7 index, 10 cycles for i5 index and 90 cycles for Read 2.

Raw sequencing data were processed using the Cell Ranger v7.1.0 FRP pipeline (10x Genomics) to generate cell-by-gene count matrices. Downstream bioinformatic analysis was performed in Python (v3.9.2) using Scanpy (v1.10.3). Quality control was applied by retaining cells with a mitochondrial gene fraction below 10%, a minimum of 200 detected genes, and a total gene count within the 2nd to 98th percentile range. Genes detected in fewer than 3 cells were excluded. Library size normalization was performed by scaling each cell to a total of 10,000 counts, followed by log2 transformation. The top 2,000 highly variable genes were identified per sample for downstream analysis. Principal component analysis (PCA) was performed on the normalized expression matrix, retaining the top 50 principal components (PCs). Batch effects were corrected by applying Harmony (v0.0.10) to the PCA-reduced embeddings. A k-nearest neighbor (kNN) graph was then constructed using the Harmony-corrected PCs with 15 neighbors. Dimensionality reduction for visualization was performed using UMAP. Unsupervised clustering was carried out across a range of resolution parameters using the Leiden algorithm (leidenalg v0.10.2) to define initial cell populations. Clusters were annotated based on canonical marker gene expression: epithelial (EPCAM, CDH1), mesenchymal (COL1A1, PDGFRA; negative for PTPRC, EPCAM, PECAM1), immune (PTPRC, CPA3, CD3D, CD68, JCHAIN, CD79A), and endothelial cells (PECAM1, CDH5; negative for PTPRC). Cellular senescence scores were calculated using the SenMayo gene set via the sc.tl.score_genes function in Scanpy.

Spatial transcriptomics using Xenium In Situ

Tissue preparation. FFPE lung tissue sections were cut at 5x 6 mm and at 5 μm thickness and mounted onto Xenium Slides according to Xenium In Situ for FFPE – Tissue Preparation Guide, CG000578, Rev C (10x genomics). The sections were underwent standard FFPE pre processing steps to enable RNA accessibility while preserving tissue morphology using Xenium In Situ for FFPE – Deparaffinization & Decrosslinking, CG000580, Rev C (10x genomics). Section morphology and tissue integrity were confirmed by pre-staining quality assessment, and regions of interest were identified in consultation with a board-certified pathologist.

The Xenium CH7CY9 probe panel, targeting approximately 389 genes, was designed by Aging Lung Lab for FFPE applications. Probe hybridization, ligation, amplification and cell segmentation staining were performed according to Xenium In Situ Gene Expression with Cell Segmentation Staining, CG000749, Rev B (10x genomics).

Automated high-resolution imaging and transcript decoding were performed on the Xenium Analyzer instrument (serial number XETG00239) using Chemistry v1, which integrates sequential hybridization readout, fluorescence imaging, and onboard spatial analysis.

Raw imaging data were processed using the Xenium Onboard Analysis pipeline and generated per cell transcript counts, spatial coordinates, and segmentation masks. Resulting datasets were explored using Xenium Explorer v4.1.1 and downstream computational analysis to characterize spatial gene expression patterns and cell–cell relationships within the lung microenvironment. All tissue acquisition and use were conducted under appropriate institutional approvals.

UNOS Registry Survival Analysis

National transplant registry data were obtained from the United Network for Organ Sharing. This study was approved by The Ohio State University Institutional Review Board (IRB No. 2018H0079). Adult recipients (≥ 18 years) undergoing lung transplantation from donation after circulatory death donors between January 1, 2010, and March 31, 2025, were included. Repeat transplants, multiorgan transplants, and ex vivo lung perfusion cases were excluded. Overall survival was defined from transplant to death and analyzed using Kaplan-Meier methods with log-rank testing. Recipients were stratified by donor and recipient age (< 60/≥60 and < 50/≥50). Survival estimates are presented with 95% confidence intervals calculated using the Greenwood method.

Statistical Analysis

In vitro experiments were repeated at least 3 times to test consistency and reliability, and representative data sets were displayed. Results are expressed as mean ± SD for each treatment group in each experiment unless otherwise indicated. Significance was determined between 2 groups using a 2-tailed Student t test or among 3 or more groups using a 1-way analysis of variance with Dunnett’s post hoc analysis to control for the familywise error rate associated with multiple comparisons of experimental treatment groups with the untreated group.

Survival analyses were performed using Kaplan–Meier methods and compared using log-rank testing. Analyses were performed using GraphPad Prism 7 software and R statistical software (Version 2025.05.1 + 513). $P < .05$ was considered statistically significant.

Abbreviations

CD38, Cluster of Differentiation 38

NAD^+, Nicotinamide adenine dinucleotide

IRI, Ischemia-reperfusion injury

SASP, Senescence-associated secretory phenotype

SA-β-gal, Senescence-associated β-galactosidase

ET-1, Endothelin-1

$CD38^{-/-}$, CD38 knockout

HUVEC, Human umbilical vein endothelial cell

H/R, Hypoxia–reoxygenation

DCD, Donation after circulatory death

DBD, Donation after brain death

BAL, Bronchoalveolar lavage

ELISA, Enzyme-linked immunosorbent assay

LDH, Lactate dehydrogenase

SDS-PAGE, Sodium dodecyl sulfate polyacrylamide gel electrophoresis

RIPA, Radioimmunoprecipitation assay

UNOS, United Network for Organ Sharing

Declarations

Funding Statement:

This research was generously supported through the NIH/NHLBI grant R01HL172490 and by the SenNet Consortium grant U54AG075931; Jewel and Frank Benson Family Endowment and The Jewel and Frank

Benson Research Professorship; The American Heart Association Postdoctoral Fellowship (Award No. 26POST1563337). The funding agency had no role in study design, data collection and analysis, decision to publish, or preparation of the manuscript.

Disclosures:

B.A.W. serves on the Clinical Events Committee of TransMedics OCS. All other authors reported no conflicts of interest.

Author Contributions:

D.D. and T.B. developed the experimental methodology, performed experiments, acquired and analyzed data, interpreted the results, prepared the figures, and drafted the manuscript. J.L.K., Y.L., and X.W. performed experimental studies, tissue processing and handling, animal experiments, data acquisition, and data analysis, and contributed to interpretation of the results. N.V.A., L.R., Y.H., and M.H. performed the single-cell and transcriptomic studies, including data generation, processing, analysis, and interpretation. D.A.G. contributed to study conception, interpretation of the findings, manuscript preparation, and critical revision of the manuscript. Q.M. contributed to the design, analysis, and interpretation of the single-cell and transcriptomic studies and provided scientific supervision. B.C. contributed to study coordination, scientific oversight, and critical revision of the manuscript. S.B. contributed to study conception and design, interpretation of the findings, scientific supervision, and critical revision of the manuscript. A.L.M. and M.R. contributed to study conception and design, experimental strategy, interpretation of the findings, scientific supervision, and critical revision of the manuscript. B.A.W. conceived and designed the study, overall study supervision, interpretation of the findings, and critical revision of the manuscript. All authors reviewed and approved the final manuscript.

Data Availability:

The data supporting the findings of this study are available from the corresponding author upon reasonable request. Source data are provided with this paper.

References

1. Valapour, M. *et al.* OPTN/SRTR 2023 Annual Data Report: Lung. *Am J Transplant* **25**, S422–s489 (2025). https://doi.org/10.1016/j.ajt.2025.01.025
2. Young, K. A. & Dilling, D. F. The Future of Lung Transplantation. *Chest* **155**, 465–473 (2019). https://doi.org/10.1016/j.chest.2018.08.1036
3. Siebiger, G. & Cypel, M. Strategies to address donor organ shortages in lung transplantation. *Curr Opin Pulm Med* (2026). https://doi.org/10.1097/mcp.0000000000001276
4. Kim, J. L. *et al.* Biometric Profiling to Quantify Lung Injury Through Ex Vivo Lung Perfusion Following Warm Ischemia. *Asaio j* **69**, e368–e375 (2023). https://doi.org/10.1097/mat.0000000000001988

5. Gouchoe, D. A. *et al.* Ex Vivo Lung Perfusion and Primary Graft Dysfunction Following Lung Transplantation: A Contemporary United Network for Organ Sharing Database Analysis. *J Clin Med* **13** (2024). https://doi.org/10.3390/jcm13154440
6. Whitson, B. A. *et al.* Risk factors for primary graft dysfunction after lung transplantation. *J Thorac Cardiovasc Surg* **131**, 73–80 (2006). https://doi.org/10.1016/j.jtcvs.2005.08.039
7. Gouchoe, D. A. *et al.* Long-Term Survival Following Primary Graft Dysfunction Development in Lung Transplantation. *J Surg Res* **296**, 47–55 (2024). https://doi.org/10.1016/j.jss.2023.12.006
8. Ferreira, L. D. *et al.* Survival Benefit of Solid-Organ Transplantation: 10-Year Update. *Dig Dis Sci* **68**, 3810–3817 (2023). https://doi.org/10.1007/s10620-023-08012-1
9. Christie, J. D., Raemdonck, D. V. & Fisher, A. J. Lung Transplantation. *New England Journal of Medicine* **391**, 1822–1836 (2024). https://doi.org/doi:10.1056/NEJMra2401039
10. Bobba, C. M. *et al.* Trends in Donation After Circulatory Death in Lung Transplantation in the United States: Impact Of Era. *Transpl Int* **35**, 10172 (2022). https://doi.org/10.3389/ti.2022.10172
11. Gouchoe, D. A. *et al.* Promoting utilization of donors after circulatory death in lung transplantation. *JHLT Open* **12**, 100491 (2026). https://doi.org/10.1016/j.jhlto.2026.100491
12. Hayasaka, K. *et al.* Aging exacerbates murine lung ischemia-reperfusion injury by excessive inflammation and impaired tissue repair response. *Am J Transplant* **24**, 293–303 (2024). https://doi.org/10.1016/j.ajt.2023.09.004
13. Iske, J. *et al.* Senolytics prevent mt-DNA-induced inflammation and promote the survival of aged organs following transplantation. *Nat Commun* **11**, 4289 (2020). https://doi.org/10.1038/s41467-020-18039-x
14. Cui, E. Y. *et al.* Outcomes of Donation After Circulatory Death Lung Transplantation in the United States Based on Procurement Strategies: A United Network for Organ Sharing Analysis. *Transplantation* (2026). https://doi.org/10.1097/tp.0000000000005803
15. Qaqish, R. *et al.* Impact of donor time to cardiac arrest in lung donation after circulatory death. *J Thorac Cardiovasc Surg* **161**, 1546–1555.e1541 (2021). https://doi.org/10.1016/j.jtcvs.2020.04.181
16. Ghaidan, H. *et al.* Reduction of primary graft dysfunction using cytokine adsorption during organ preservation and after lung transplantation. *Nat Commun* **13**, 4173 (2022). https://doi.org/10.1038/s41467-022-31811-5
17. Gouchoe, D. A. *et al.* Ex Vivo Lung Perfusion in Donation After Cardiac and Brain Death Donation. *Ann Thorac Surg* **119**, 651–659 (2025). https://doi.org/10.1016/j.athoracsur.2024.11.008
18. Chacon-Alberty, L. *et al.* Primary Graft Dysfunction in Lung Transplantation: A Review of Mechanisms and Future Applications. *Transplantation* **107**, 1687–1697 (2023). https://doi.org/10.1097/tp.0000000000004503
19. Eltzschig, H. K. & Eckle, T. Ischemia and reperfusion--from mechanism to translation. *Nat Med* **17**, 1391–1401 (2011). https://doi.org/10.1038/nm.2507

20. Zhou, W.-c., Qu, J., Xie, S.-y., Sun, Y. & Yao, H.-w. Mitochondrial Dysfunction in Chronic Respiratory Diseases: Implications for the Pathogenesis and Potential Therapeutics. *Oxidative Medicine and Cellular Longevity* **2021**, 5188306 (2021). https://doi.org/https://doi.org/10.1155/2021/5188306
21. Parikh, P. *et al.* Cellular senescence in the lung across the age spectrum. *Am J Physiol Lung Cell Mol Physiol* **316**, L826–l842 (2019). https://doi.org/10.1152/ajplung.00424.2018
22. Dugbartey, G. J. Cellular and molecular mechanisms of cell damage and cell death in ischemia-reperfusion injury in organ transplantation. *Mol Biol Rep* **51**, 473 (2024). https://doi.org/10.1007/s11033-024-09261-7
23. Pan, J., Zhang, J. & Lu, X. Incidence of primary graft dysfunction and its associated risk factors after lung transplantation: a systematic review and meta-analysis. *Surg Today* **55**, 1783–1802 (2025). https://doi.org/10.1007/s00595-025-03129-4
24. Christie, J. D. *et al.* Impact of primary graft failure on outcomes following lung transplantation. *Chest* **127**, 161–165 (2005). https://doi.org/10.1378/chest.127.1.161
25. Cerier, E. *et al.* Temporal correlation between postreperfusion complement deposition and severe primary graft dysfunction in lung allografts. *Am J Transplant* **24**, 577–590 (2024). https://doi.org/10.1016/j.ajt.2023.11.006
26. Verleden, S. E., Vos, R., Vanaudenaerde, B. M. & Verleden, G. M. Chronic lung allograft dysfunction phenotypes and treatment. *J Thorac Dis* **9**, 2650–2659 (2017). https://doi.org/10.21037/jtd.2017.07.81
27. Mammoto, A. *et al.* Control of lung vascular permeability and endotoxin-induced pulmonary oedema by changes in extracellular matrix mechanics. *Nat Commun* **4**, 1759 (2013). https://doi.org/10.1038/ncomms2774
28. Klak, I., Ptak-Belowska, A. & Krzysiek-Maczka, G. Cellular senescence: Between protection and pathologies. *J Physiol Pharmacol* **77**, 3–14 (2026). https://doi.org/10.26402/jpp.2026.1.01
29. Basilicata, M. G. *et al.* Multi-omics strategies to decode the molecular landscape of cellular senescence. *Ageing Res Rev* **111**, 102824 (2025). https://doi.org/10.1016/j.arr.2025.102824
30. Zanders, L., Arifaj, D., Wagner, J. U. G. & Dimmeler, S. Cellular Senescence, Inflammaging and Cardiovascular Disease. *Immunological Reviews* **337**, e70084 (2026). https://doi.org/https://doi.org/10.1111/imr.70084
31. Barnes, P. J., Baker, J. & Donnelly, L. E. Cellular Senescence as a Mechanism and Target in Chronic Lung Diseases. *Am J Respir Crit Care Med* **200**, 556–564 (2019). https://doi.org/10.1164/rccm.201810-1975TR
32. Bisht, K. *et al.* Immunomodulatory properties of CD38 antibodies and their effect on anticancer efficacy in multiple myeloma. *Cancer Medicine* **12**, 20332–20352 (2023). https://doi.org/https://doi.org/10.1002/cam4.6619
33. Malavasi, F. *et al.* Evolution and function of the ADP ribosyl cyclase/CD38 gene family in physiology and pathology. *Physiol Rev* **88**, 841–886 (2008). https://doi.org/10.1152/physrev.00035.2007

34. Lee, H. C., Deng, Q. W. & Zhao, Y. J. The calcium signaling enzyme CD38 - a paradigm for membrane topology defining distinct protein functions. *Cell Calcium* **101**, 102514 (2022). https://doi.org/10.1016/j.ceca.2021.102514
35. Partida-Sánchez, S. *et al.* Cyclic ADP-ribose production by CD38 regulates intracellular calcium release, extracellular calcium influx and chemotaxis in neutrophils and is required for bacterial clearance in vivo. *Nature Medicine* **7**, 1209–1216 (2001). https://doi.org/10.1038/nm1101-1209
36. van de Donk, N. W. C. J. *et al.* Monoclonal antibodies targeting CD38 in hematological malignancies and beyond. *Immunological Reviews* **270**, 95–112 (2016). https://doi.org/https://doi.org/10.1111/imr.12389
37. Camacho-Pereira, J. *et al.* CD38 Dictates Age-Related NAD Decline and Mitochondrial Dysfunction through an SIRT3-Dependent Mechanism. *Cell Metab* **23**, 1127–1139 (2016). https://doi.org/10.1016/j.cmet.2016.05.006
38. Covarrubias, A. J. *et al.* Senescent cells promote tissue NAD(+) decline during ageing via the activation of CD38(+) macrophages. *Nat Metab* **2**, 1265–1283 (2020). https://doi.org/10.1038/s42255-020-00305-3
39. Zhao, Q. H. *et al.* Myeloid but not hepatocytic CD38 is a key driver for hepatic ischemia/reperfusion injury. *Signal Transduct Target Ther* **10**, 150 (2025). https://doi.org/10.1038/s41392-025-02233-8
40. Gomes, A. P. *et al.* Declining NAD(+) induces a pseudohypoxic state disrupting nuclear-mitochondrial communication during aging. *Cell* **155**, 1624–1638 (2013). https://doi.org/10.1016/j.cell.2013.11.037
41. Gouchoe, D. A. *et al.* The role of CD38 in ischemia reperfusion injury in cardiopulmonary bypass and thoracic transplantation: a narrative review. *J Thorac Dis* **15**, 5736–5749 (2023). https://doi.org/10.21037/jtd-23-725
42. Gielis, J. F. *et al.* A murine model of lung ischemia and reperfusion injury: tricks of the trade. *J Surg Res* **194**, 659–666 (2015). https://doi.org/10.1016/j.jss.2014.12.008
43. Haffner, C. D. *et al.* Discovery, Synthesis, and Biological Evaluation of Thiazoloquin(az)olin(on)es as Potent CD38 Inhibitors. *J Med Chem* **58**, 3548–3571 (2015). https://doi.org/10.1021/jm502009h
44. Boslett, J., Hemann, C., Christofi, F. L. & Zweier, J. L. Characterization of CD38 in the major cell types of the heart: endothelial cells highly express CD38 with activation by hypoxia-reoxygenation triggering NAD(P)H depletion. *Am J Physiol Cell Physiol* **314**, C297–c309 (2018). https://doi.org/10.1152/ajpcell.00139.2017
45. Escande, C. *et al.* Flavonoid apigenin is an inhibitor of the NAD+ ase CD38: implications for cellular NAD+ metabolism, protein acetylation, and treatment of metabolic syndrome. *Diabetes* **62**, 1084–1093 (2013). https://doi.org/10.2337/db12-1139
46. Kellenberger, E., Kuhn, I., Schuber, F. & Muller-Steffner, H. Flavonoids as inhibitors of human CD38. *Bioorg Med Chem Lett* **21**, 3939–3942 (2011). https://doi.org/10.1016/j.bmcl.2011.05.022
47. Zhu, Y. *et al.* New agents that target senescent cells: the flavone, fisetin, and the BCL-X(L) inhibitors, A1331852 and A1155463. *Aging (Albany NY)* **9**, 955–963 (2017).

https://doi.org/10.18632/aging.101202

48. Shu, B. *et al.* Blockade of CD38 diminishes lipopolysaccharide-induced macrophage classical activation and acute kidney injury involving NF-κB signaling suppression. *Cell Signal* **42**, 249–258 (2018). https://doi.org/10.1016/j.cellsig.2017.10.014
49. Wang, L. F. *et al.* CD38 Deficiency Alleviates D-Galactose-Induced Myocardial Cell Senescence Through NAD(+)/Sirt1 Signaling Pathway. *Front Physiol* **10**, 1125 (2019). https://doi.org/10.3389/fphys.2019.01125
50. Fang, E. F. *et al.* NAD(+) augmentation restores mitophagy and limits accelerated aging in Werner syndrome. *Nat Commun* **10**, 5284 (2019). https://doi.org/10.1038/s41467-019-13172-8
51. Griffiths, H. B. S., Williams, C., King, S. J. & Allison, S. J. Nicotinamide adenine dinucleotide (NAD+): essential redox metabolite, co-substrate and an anti-cancer and anti-ageing therapeutic target. *Biochem Soc Trans* **48**, 733–744 (2020). https://doi.org/10.1042/bst20190033
52. Chini, C. *et al.* The NADase CD38 is induced by factors secreted from senescent cells providing a potential link between senescence and age-related cellular NAD(+) decline. *Biochem Biophys Res Commun* **513**, 486–493 (2019). https://doi.org/10.1016/j.bbrc.2019.03.199
53. Van Raemdonck, D. *et al.* Donation after circulatory death in lung transplantation-five-year follow-up from ISHLT Registry. *J Heart Lung Transplant* **38**, 1235–1245 (2019). https://doi.org/10.1016/j.healun.2019.09.007
54. Levin, E. R. Endothelins. *New England Journal of Medicine* **333**, 356–363 (1995). https://doi.org/doi:10.1056/NEJM199508103330607
55. Mitsuoka, H. *et al.* Contribution of endothelin-1 to microcirculatory impairment in total hepatic ischemia and reperfusion injury. *Transplantation* **67**, 514–520 (1999). https://doi.org/10.1097/00007890-199902270-00004
56. Niu, J., Wu, J., Li, X. & Zhang, F. Association between endothelin-1/endothelin receptor A and inflammation in mouse kidneys following acute ischemia/reperfusion. *Mol Med Rep* **11**, 3981–3987 (2015). https://doi.org/10.3892/mmr.2014.3138
57. Gouchoe, D. A. *et al.* MG53 mitigates warm ischemic lung injury in a murine model of transplantation. *J Thorac Cardiovasc Surg* **168**, e13–e26 (2024). https://doi.org/10.1016/j.jtcvs.2023.10.056
58. Donato, A. J. *et al.* Vascular endothelial dysfunction with aging: endothelin-1 and endothelial nitric oxide synthase. *Am J Physiol Heart Circ Physiol* **297**, H425–432 (2009). https://doi.org/10.1152/ajpheart.00689.2008
59. Goel, A. *et al.* Increased endothelial exocytosis and generation of endothelin-1 contributes to constriction of aged arteries. *Circ Res* **107**, 242–251 (2010). https://doi.org/10.1161/circresaha.109.210229
60. Liao, W. I. *et al.* A Mouse Model of Orotracheal Intubation and Ventilated Lung Ischemia Reperfusion Surgery. *J Vis Exp* (2022). https://doi.org/10.3791/64383

Figures

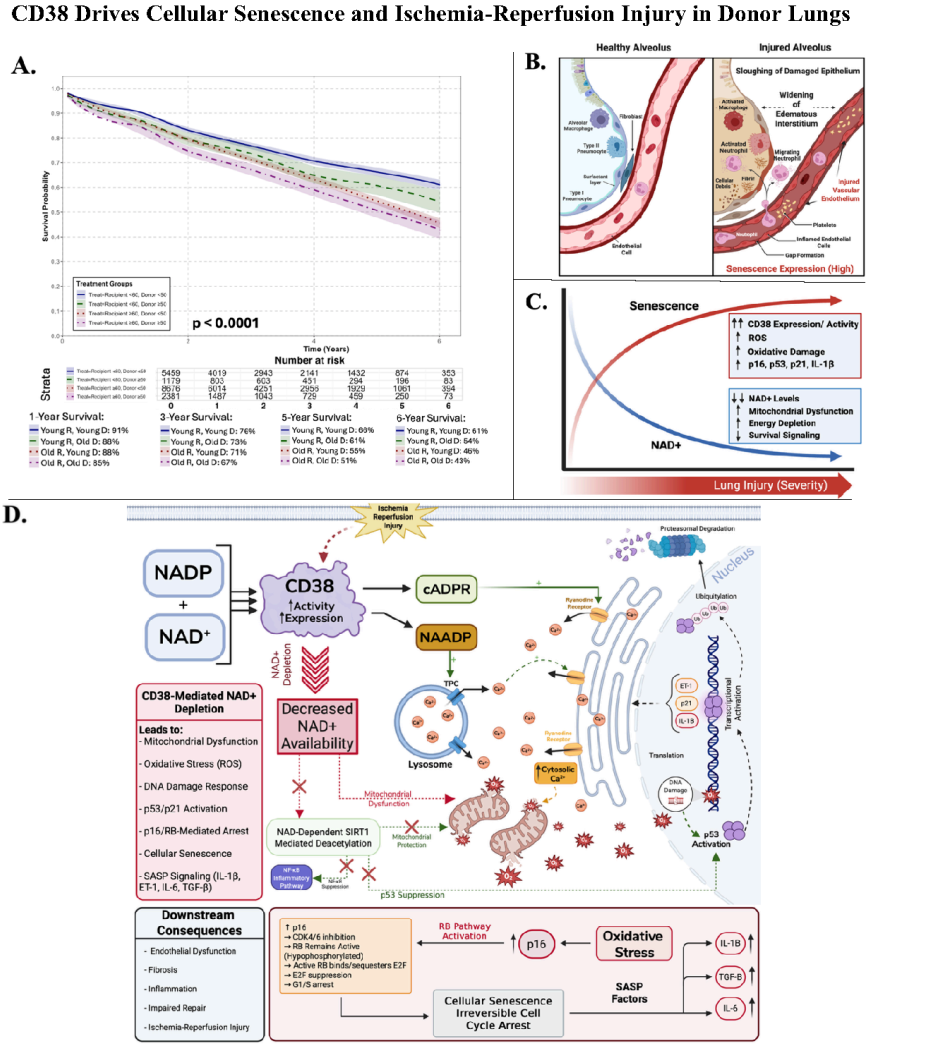

Figure 1. Donor Aging, Cellular Senescence, and CD38-Mediated NAD⁺ Depletion Contribute to Lung Transplant Injury and Reduced Survival
1A. Kaplan-Meier survival analysis of adult first-time lung transplant recipients in the United Network for Organ Sharing (UNOS) registry between 2019-2025; n=17,695, stratified into four donor-recipient groups: young recipient/young donor (recipient <60 years, donor <50 years; n=5,459), younger recipient/older donor (recipient <60 years, donor ≥50 years; n=1,179), older recipient/younger donor (recipient ≥60 years, donor <50 years; n=8,676), and older recipient/older donor (recipient ≥60 years, donor ≥50 years; n=2,381). **1B.** Schematic comparison of the healthy and injured alveolar microenvironment demonstrating the emergence of cellular senescence during lung injury. **1C.** Schematic demonstrating the progressive relationship between increasing cellular senescence, CD38 activity, oxidative and inflammatory signaling, NAD⁺ depletion, and worsening lung injury severity. **1D.** CD38-mediated NAD⁺ depletion and calcium-dependent senescence signaling. CD38 catalyzes NAD⁺-consuming reactions that generate ADPR through NAD⁺ glycohydrolase activity and cADPR through ADP-ribosyl cyclase activity. CD38 also catalyzes a base-exchange reaction in which NADP⁺ and nicotinic acid are used to generate NAADP. cADPR and NAADP promote Ca^{2+} mobilization from distinct intracellular stores, with cADPR primarily linked to endoplasmic reticulum calcium stores and NAADP linked to acidic/endolysosomal calcium stores. Together, CD38-mediated NAD⁺ depletion, calcium signaling, and oxidative stress activate senescence-associated pathways, including p53/p21 and p16 signaling, contributing to cellular senescence. This pathway provides a mechanistic link between metabolic dysfunction, inflammatory signaling, and cellular senescence in donor lungs exposed to aging and ischemic stress.

Figure 1

See image above for figure legend.

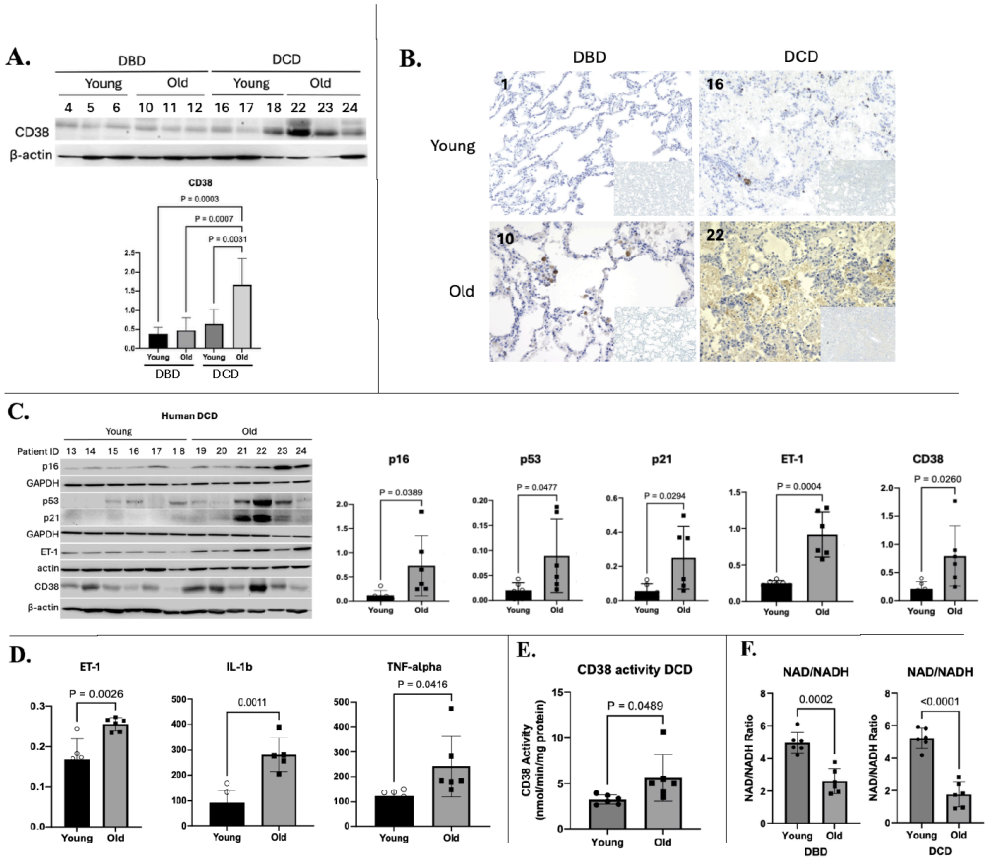

Figure 2. Donor Aging and Ischemic Stress are Associated with Increased CD38 Expression and Senescence Signaling in Human Donor Lungs.

2A. Representative Western blot and corresponding densitometric quantification of CD38 expression in human donor lungs stratified by donor type and donor age. Protein expression was normalized to β-actin. Data are presented as mean ± SEM. Comparisons performed using two-way ANOVA with donor type and donor age as factors, followed by post hoc multiple-comparison testing. **2B.** Representative immunohistochemical staining for CD38 in human donor lungs stratified by donor age and donor type. Insets demonstrate corresponding low-magnification views. **2C.** Representative Western blots and corresponding densitometric quantification of p16, p53, p21, ET-1, and CD38 expression in human DCD donor lungs stratified by donor age. Protein expression was normalized to GAPDH, actin, or β-actin as indicated. Data are presented as mean ± SEM. Comparisons performed using unpaired Student's t-test. **2D.** Quantification of ET-1, IL-1β, and TNF-α in human DCD donor lungs stratified by donor age. Data are presented as mean ± SEM. Comparisons were performed using unpaired Student's t-test. **2E.** Quantification of CD38 enzymatic activity in human DCD donor lungs stratified by donor age. Data are presented as mean ± SEM. Comparisons were performed using unpaired Student's t-test. **2F.** Quantification of NAD/NADH ratios in human donor lungs stratified by donor type and donor age. Data are presented as mean ± SEM. Statistical analysis was performed using two-way ANOVA with donor age and donor type as factors, followed by post hoc multiple-comparison testing.

Figure 2

See image above for figure legend.

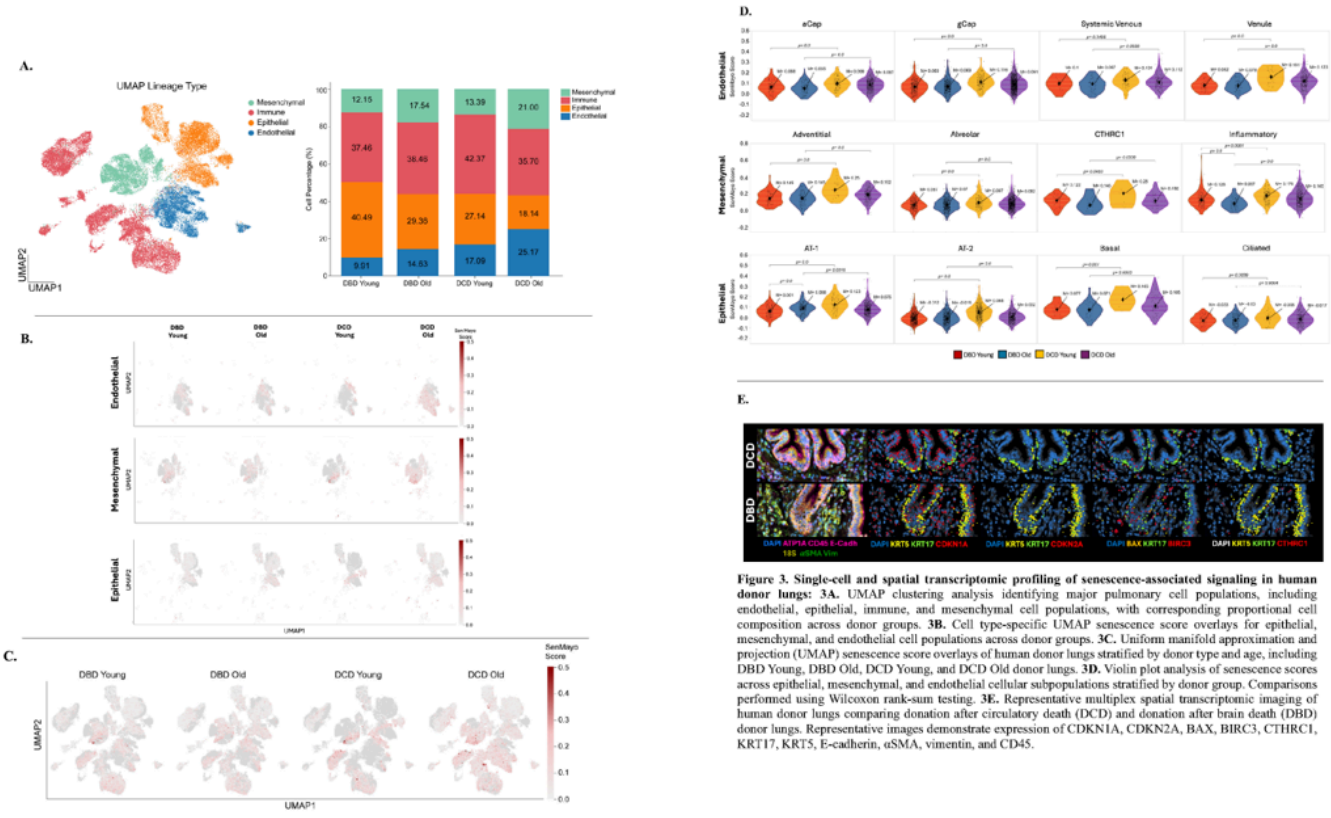

Figure 3. Single-cell and spatial transcriptomic profiling of senescence-associated signaling in human donor lungs: 3A. UMAP clustering analysis identifying major pulmonary cell populations, including endothelial, epithelial, immune, and mesenchymal cell populations, with corresponding proportional cell composition across donor groups. **3B.** Cell type-specific UMAP senescence score overlays for epithelial, mesenchymal, and endothelial cell populations across donor groups. **3C.** Uniform manifold approximation and projection (UMAP) senescence score overlays of human donor lungs stratified by donor type and age, including DBD Young, DBD Old, DCD Young, and DCD Old donor lungs. **3D.** Violin plot analysis of senescence scores across epithelial, mesenchymal, and endothelial cellular subpopulations stratified by donor group. Comparisons performed using Wilcoxon rank-sum testing. **3E.** Representative multiplex spatial transcriptomic imaging of human donor lungs comparing donation after circulatory death (DCD) and donation after brain death (DBD) donor lungs. Representative images demonstrate expression of CDKN1A, CDKN2A, BAX, BIRC3, CTHRC1, KRT17, KRT5, E-cadherin, αSMA, vimentin, and CD45.

Figure 3

See image above for figure legend.

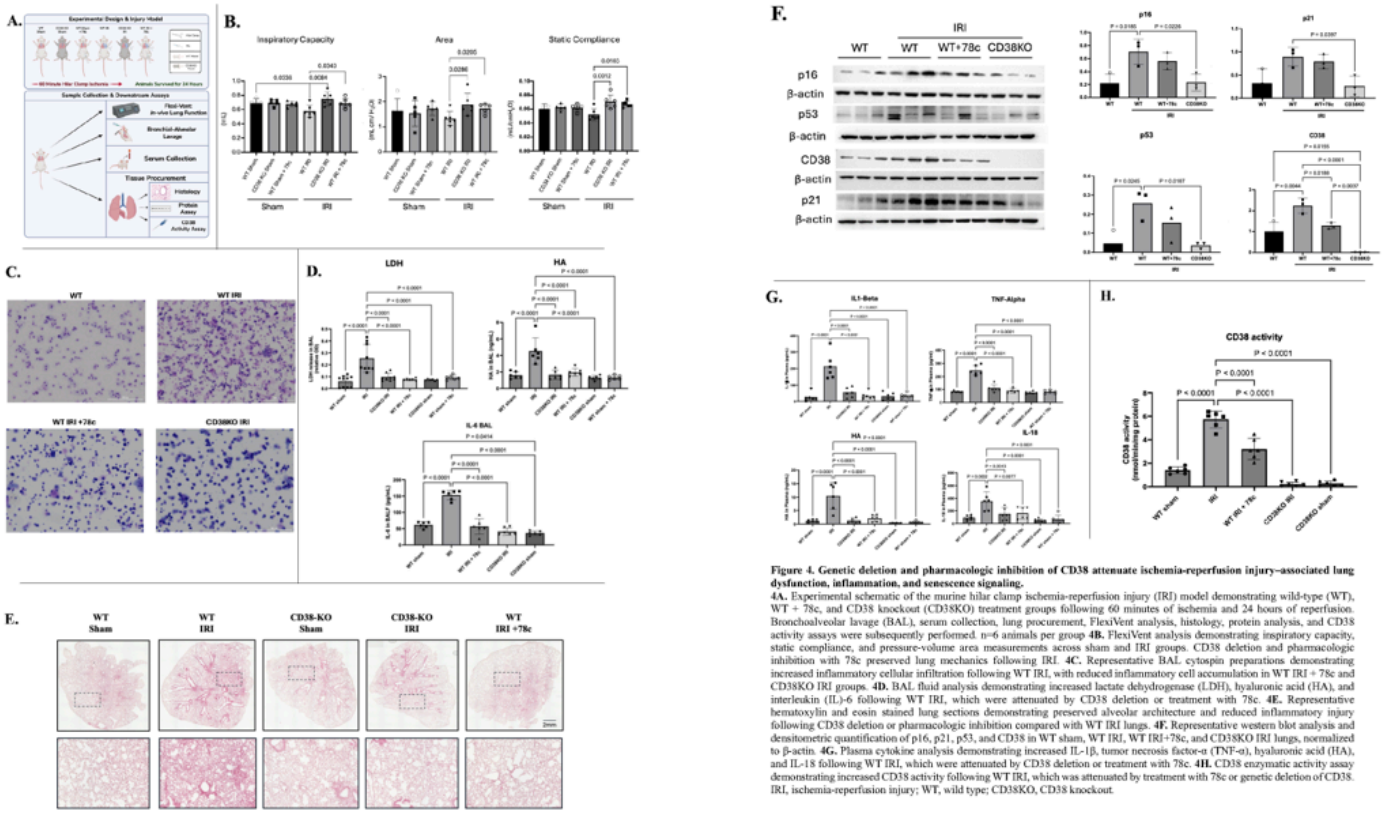

Figure 4. Genetic deletion and pharmacologic inhibition of CD38 attenuate ischemia-reperfusion injury–associated lung dysfunction, inflammation, and senescence signaling.

4A. Experimental schematic of the murine hilar clamp ischemia-reperfusion injury (IRI) model demonstrating wild-type (WT), WT + 78c, and CD38 knockout (CD38KO) treatment groups following 60 minutes of ischemia and 24 hours of reperfusion. Bronchoalveolar lavage (BAL), serum collection, lung procurement, FlexiVent analysis, histology, protein analysis, and CD38 activity assays were subsequently performed. n=6 animals per group **4B.** FlexiVent analysis demonstrating inspiratory capacity, static compliance, and pressure-volume area measurements across sham and IRI groups. CD38 deletion and pharmacologic inhibition with 78c preserved lung mechanics following IRI. **4C.** Representative BAL cytospin preparations demonstrating increased inflammatory cellular infiltration following WT IRI, with reduced inflammatory cell accumulation in WT IRI + 78c and CD38KO IRI groups. **4D.** BAL fluid analysis demonstrating increased lactate dehydrogenase (LDH), hyaluronic acid (HA), and interleukin (IL)-6 following WT IRI, which were attenuated by CD38 deletion or treatment with 78c. **4E.** Representative hematoxylin and eosin stained lung sections demonstrating preserved alveolar architecture and reduced inflammatory injury following CD38 deletion or pharmacologic inhibition compared with WT IRI lungs. **4F.** Representative western blot analysis and densitometric quantification of p16, p21, p53, and CD38 in WT sham, WT IRI, WT IRI+78c, and CD38KO IRI lungs, normalized to β-actin. **4G.** Plasma cytokine analysis demonstrating increased IL-1β, tumor necrosis factor-α (TNF-α), hyaluronic acid (HA), and IL-18 following WT IRI, which were attenuated by CD38 deletion or treatment with 78c. **4H.** CD38 enzymatic activity assay demonstrating increased CD38 activity following WT IRI, which was attenuated by treatment with 78c or genetic deletion of CD38. IRI, ischemia-reperfusion injury; WT, wild type; CD38KO, CD38 knockout.

Figure 4

See image above for figure legend.

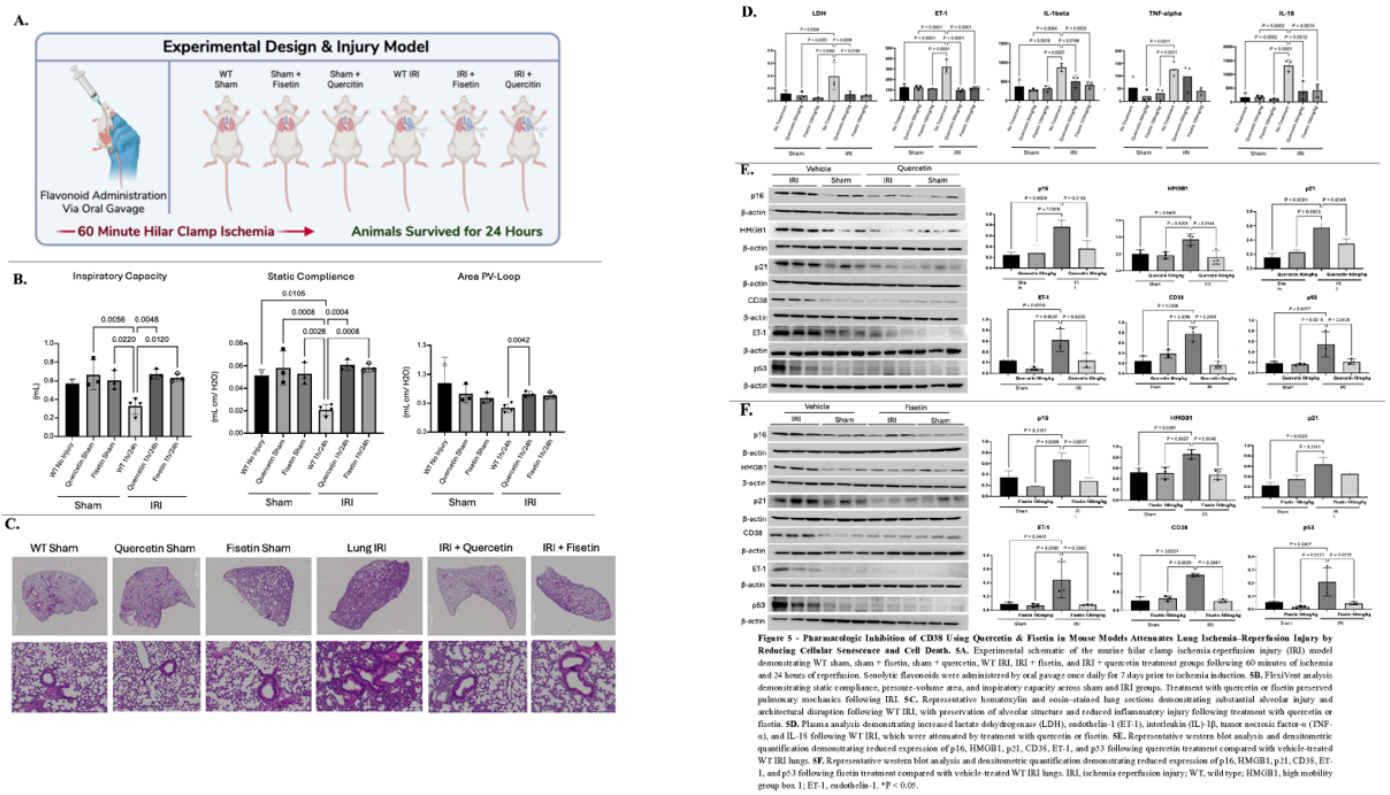

Figure 5 - Pharmacologic Inhibition of CD38 Using Quercetin & Fisetin in Mouse Models Attenuates Lung Ischemia–Reperfusion Injury by Reducing Cellular Senescence and Cell Death. 5A. Experimental schematic of the murine hilar clamp ischemia-reperfusion injury (IRI) model demonstrating WT sham, sham + fisetin, sham + quercetin, WT IRI, IRI + fisetin, and IRI + quercetin treatment groups following 60 minutes of ischemia and 24 hours of reperfusion. Senolytic flavonoids were administered by oral gavage once daily for 7 days prior to ischemia induction. **5B.** FlexiVent analysis demonstrating static compliance, pressure-volume area, and inspiratory capacity across sham and IRI groups. Treatment with quercetin or fisetin preserved pulmonary mechanics following IRI. **5C.** Representative hematoxylin and eosin–stained lung sections demonstrating substantial alveolar injury and architectural disruption following WT IRI, with preservation of alveolar structure and reduced inflammatory injury following treatment with quercetin or fisetin. **5D.** Plasma analysis demonstrating increased lactate dehydrogenase (LDH), endothelin-1 (ET-1), interleukin (IL)-1β, tumor necrosis factor-α (TNF-α), and IL-18 following WT IRI, which were attenuated by treatment with quercetin or fisetin. **5E.** Representative western blot analysis and densitometric quantification demonstrating reduced expression of p16, HMGB1, p21, CD38, ET-1, and p53 following quercetin treatment compared with vehicle-treated WT IRI lungs. **5F.** Representative western blot analysis and densitometric quantification demonstrating reduced expression of p16, HMGB1, p21, CD38, ET-1, and p53 following fisetin treatment compared with vehicle-treated WT IRI lungs. IRI, ischemia-reperfusion injury; WT, wild type; HMGB1, high mobility group box 1; ET-1, endothelin-1. *P < 0.05.

Figure 5

See image above for figure legend.

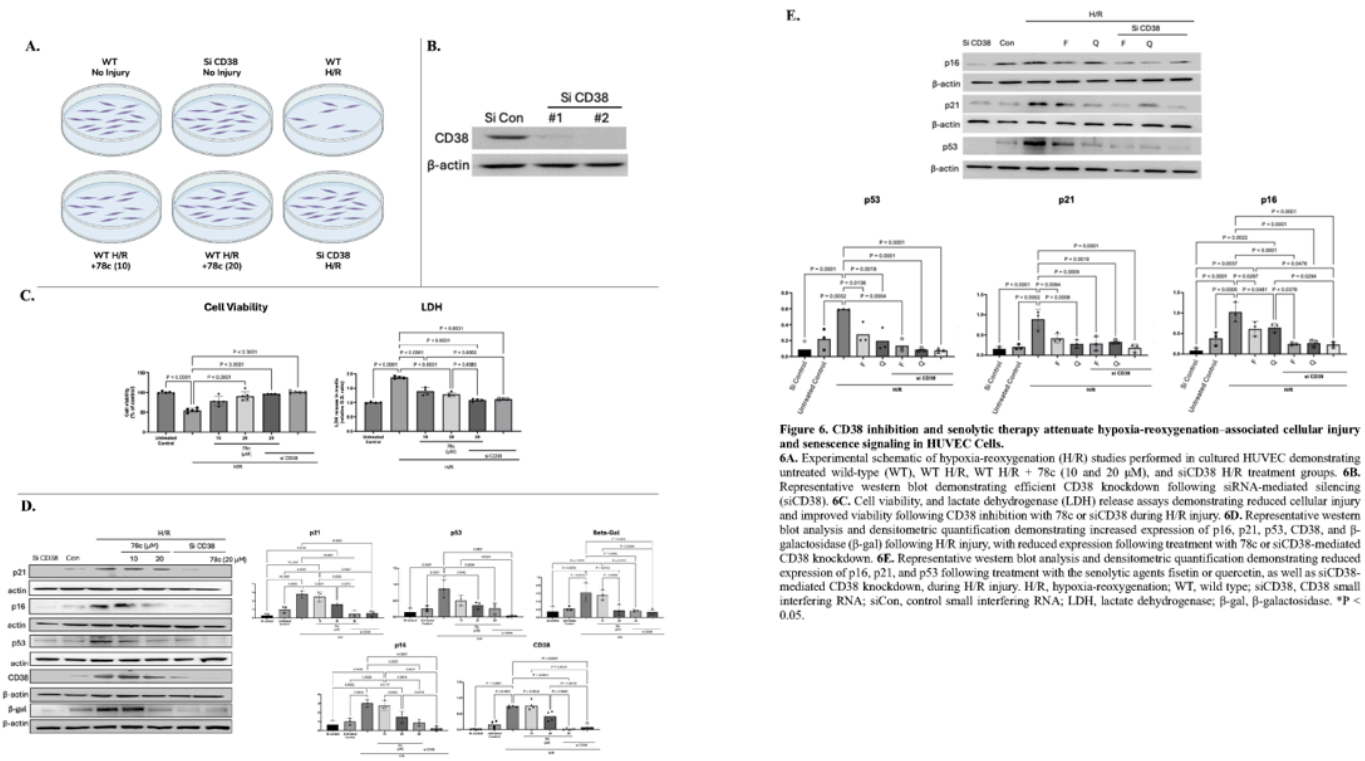

Figure 6. CD38 inhibition and senolytic therapy attenuate hypoxia-reoxygenation–associated cellular injury and senescence signaling in HUVEC Cells.

6A. Experimental schematic of hypoxia-reoxygenation (H/R) studies performed in cultured HUVEC demonstrating untreated wild-type (WT), WT H/R, WT H/R + 78c (10 and 20 μM), and siCD38 H/R treatment groups. **6B.** Representative western blot demonstrating efficient CD38 knockdown following siRNA-mediated silencing (siCD38). **6C.** Cell viability, and lactate dehydrogenase (LDH) release assays demonstrating reduced cellular injury and improved viability following CD38 inhibition with 78c or siCD38 during H/R injury. **6D.** Representative western blot analysis and densitometric quantification demonstrating increased expression of p16, p21, p53, CD38, and β-galactosidase (β-gal) following H/R injury, with reduced expression following treatment with 78c or siCD38-mediated CD38 knockdown. **6E.** Representative western blot analysis and densitometric quantification demonstrating reduced expression of p16, p21, and p53 following treatment with the senolytic agents fisetin or quercetin, as well as siCD38-mediated CD38 knockdown, during H/R injury. H/R, hypoxia-reoxygenation; WT, wild type; siCD38, CD38 small interfering RNA; siCon, control small interfering RNA; LDH, lactate dehydrogenase; β-gal, β-galactosidase. *P < 0.05.

Figure 6

See image above for figure legend.